International Journal of Adhesion & Adhesives 37 (2012) 3–10

Contents lists available at SciVerse ScienceDirect

International Journal of Adhesion & Adhesives

journal homepage: www.elsevier.com/locate/ijadhadh

Investigating tensile behaviour of toughened epoxy paste adhesives using circumferentially notched cylindrical bulk specimens

K.B. Katnam *, A.J. Comer, W.F. Stanley, M. Buggy, T.M. Young

Irish Centre for Composites Research (IComp), Materials and Surface Science Institute (MSSI), University of Limerick, Limerick, Ireland

ARTICLE INFO

Available online 21 January 2012

Keywords:
Epoxy/epoxides
Destructive testing
Microscopy
Mechanical properties of adhesives
Hollow glass microspheres

ABSTRACT

Toughened epoxy adhesives are frequently used to bond metals and polymer-matrix composite materials in many structural applications. The mechanical properties of adhesives are often characterised by testing either bulk adhesive specimens or bonded joints (*i.e. in-situ* form). In this paper, cylindrical bulk specimens with circumferential notches were manufactured and tested to investigate the tensile behaviour of an epoxy paste adhesive toughened with hollow glass microspheres. Bulk specimens were manufactured from the paste adhesive using injection moulding. Tensile tests were conducted for strain-rate and stress triaxiality effects by varying displacement rates and notch radii, respectively. Fracture surfaces were examined using optical and scanning electron microscopy to identify failure mechanisms. The results obtained from the toughened paste adhesive indicate that strain-rate and stress triaxiality influence its tensile fracture behaviour.

1. Introduction

Epoxy adhesives are often used in structural applications for bonding primary and secondary structural components. For example, in the aeronautical industry [1], the main use of structural adhesives is in bonding internal structural elements (*e.g.* stringers) to skins in fuselages, wings, ailerons, *etc.* The strength of adhesively bonded joints primarily depends on the mechanical properties of adherend, adhesive and adherend–adhesive interface [2,3].

To characterise the mechanical properties of adhesives, experimental tests are performed on either bulk adhesive specimens or bonded joints (*i.e. in-situ* form). To compare the mechanical properties of the bulk material form with the in-situ material form, research studies [4–8] have been conducted and found that the mechanical behaviour of the two forms are similar. On the contrary, it has also been observed that the variation in adhesive bondline thickness influences the strength of bonded joints, which is often related to the *in-situ* material behaviour (*i.e.* with constrained process zones [9,10] and triaxial stress states [11,12]). It is not yet fully understood whether the mechanical properties of adhesives can accurately be determined by testing either bulk specimens or bonded joints. In addition, second-phase particles, *e.g.* glass microspheres [13–16], are often used to toughen epoxy adhesives—making it more difficult to accurately determine the mechanical properties of toughened adhesives.

It is often seen that the mechanical behaviour of epoxy adhesives, being polymers, are sensitive to strain rates [17–19] and triaxial stress states [20–23]. Moreover, to model and accurately predict the mechanical behaviour of adhesively bonded joints [24], experimental characterisation of bulk adhesive for different strain-rates and triaxial stress states is important. In this regard, a two-part toughened paste adhesive was considered for the current study to investigate the tensile fracture behaviour for different strain rates and tri-axial stress states. The objectives of the study were to: (a) develop a novel manufacturing process and a test setup to cure and test cylindrical bulk specimens from paste adhesives, (b) investigate the tensile fracture behaviour of a toughened epoxy adhesive as a function of strain-rate and stress triaxiality and (c) examine the failure mechanisms involved.

Cylindrical bulk specimens were manufactured by injecting uncured paste adhesive into a two-part mould—this approach can, in general, be used to manufacture bulk specimens from paste adhesives. Tensile tests were performed on circumferentially notched cylindrical specimens [25–27] for different notch radii and displacement rates. Furthermore, fracture surfaces were examined using optical and scanning electron microscopy to identify failure mechanisms. The results obtained from the toughened paste adhesive indicate that strain-rate and stress triaxiality influence its tensile fracture behaviour, which may consequently influence the fracture behaviour of bonded joints.

2. Materials and manufacturing

2.1. Two-part epoxy adhesive

A two-part toughened epoxy paste adhesive—a research grade structural adhesive for aerospace applications—was used to

* Corresponding author. Tel.: +353 61202253; fax: +353 61202944.
E-mail address: Kali-Babu.Katnam@ul.ie (K.B. Katnam).

0143-7496/$ - see front matter © 2012 Elsevier Ltd. All rights reserved.
doi:10.1016/j.ijadhadh.2012.01.007

manufacture bulk specimens. Hollow glass microspheres of different sizes are added in the adhesive to improve its toughness by the manufacturer. The adhesive was supplied by the manufacturer in a dual cartridge form. For the current study, a dispenser-mix technique was employed to manufacture bulk adhesive specimens. The dispenser was loaded with a dual cartridge and a static mixer, and compressed air was pumped into the system to get a uniform adhesive paste from the nozzle of the static mixer.

2.2. Adhesive injection and curing

To manufacture cylindrical bulk adhesive specimens, a two-part mould was designed with stepped cylindrical grooves—the top and bottom moulds are shown in Fig. 1a. The mould was designed to manufacture five specimens at a time. The dimensions of each stepped cylindrical groove were chosen to cure cylindrical specimens with 40 mm in length and 5 mm in radius (see Fig. 1b). Moreover, hollow aluminium cylinders (30 mm length, 10 mm external radius and 5 mm internal radius) with internal threads were used in the manufacture process (see Fig. 1c). A release agent was applied to the stepped cylindrical grooves to prevent adhesion. The two hollow cylinders were located in each stepped cylindrical groove and the top and bottom moulds were closed. The adhesive was then injected into each groove from one end, as shown in Fig. 2, to minimise air entrapment and void formation. Furthermore, the nozzle of the static mixer was cut to increase the adhesive bead size to match the diameter of the cylindrical specimens to avoid rheological issues (*e.g.* tensile fracture of the uncured adhesive). The adhesive was cured at 80 °C for 4 h in an oven (Binder ED23).

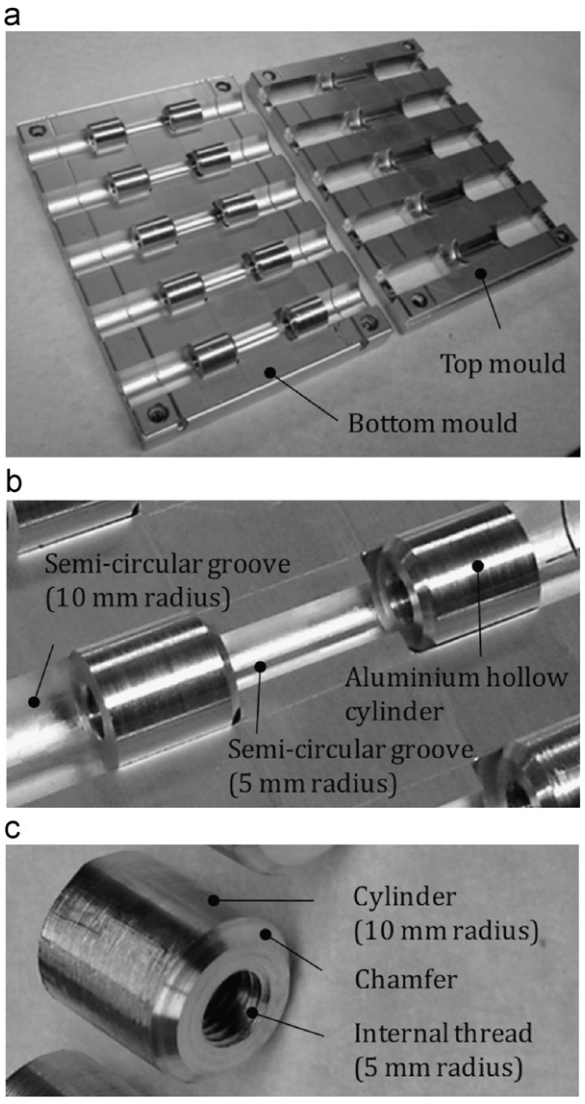

Fig. 1. Manufacturing tools: (a) top and bottom aluminium moulds, (b) stepped semi-circular grooves to accommodate aluminium hollow cylinders and (c) aluminium hollow cylinder with internal thread.

2.3. Bulk specimens

To produce circumferentially notched specimens, the cured specimens were notched using a lathe machine [28]. Notch tip radius was varied and four different specimens were manufactured (see Fig. 3). The dimensional details (in mm) of the bulk specimens are shown in Fig. 4. The notch geometry was varied to induce failure at different triaxial stress states. The V-notch was introduced with a radius of approximately 0.02 mm and a V-angle of 60°. In all the specimens, the radius of the cylindrical specimens at the notched region was reduced to 3 mm from 5 mm (see Fig. 4).

3. Numerical modelling

To calculate the stress concentration factors and the stress triaxiality values in the manufactured bulk specimens, axisymmetric finite element models were used and quasi-static stress analyses were performed for different notch geometries using axisymmetric elements (CAX4R, 4 node bilinear elements with

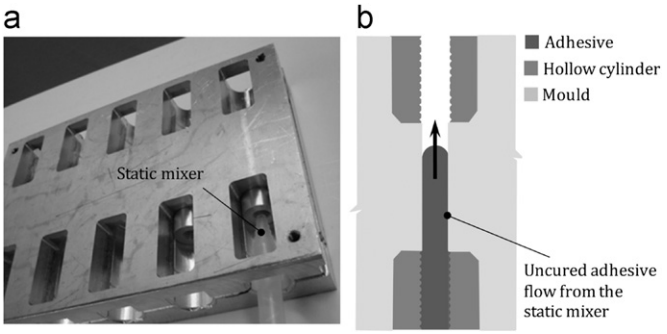

Fig. 2. Curing bulk specimens: (a) adhesive injection using a static mixer and (b) a schematic showing uncured adhesive flow.

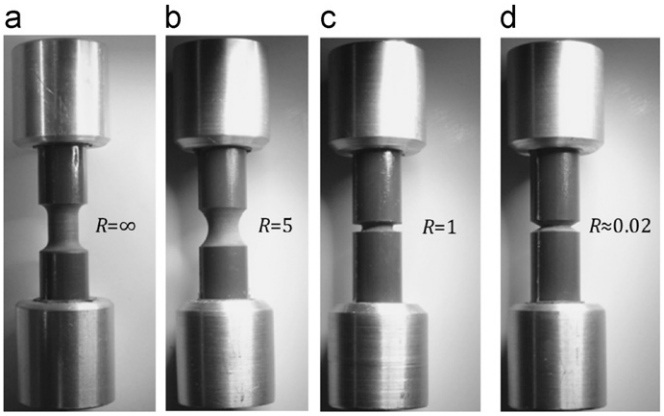

Fig. 3. Circumferentially notched cylindrical specimens with different notch tip geometries ($R=\infty$, R=5 mm, $R=1$ mm and $R \approx 0.02$ mm).

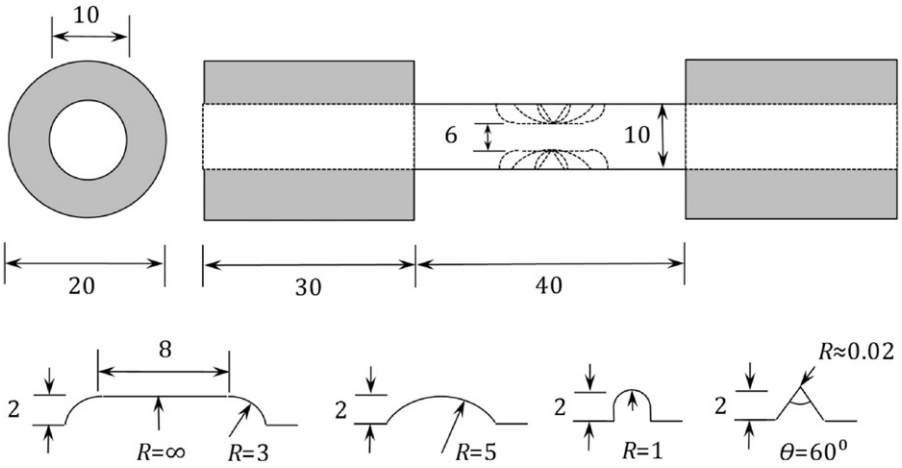

Fig. 4. Dimensional details of bulk adhesive specimens with different notch tip geometries (All dimensions are in mm).

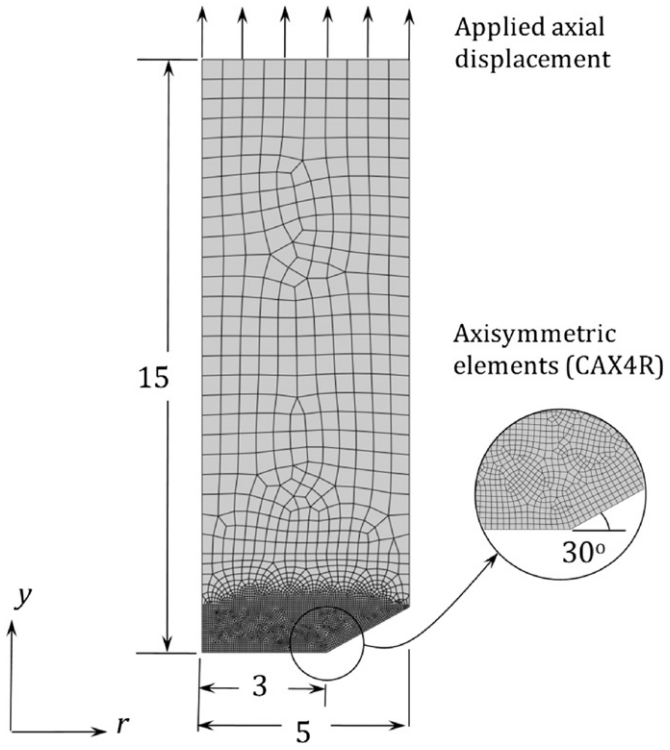

Fig. 5. Axisymmetric model for the V-notch specimen (dimensions in mm).

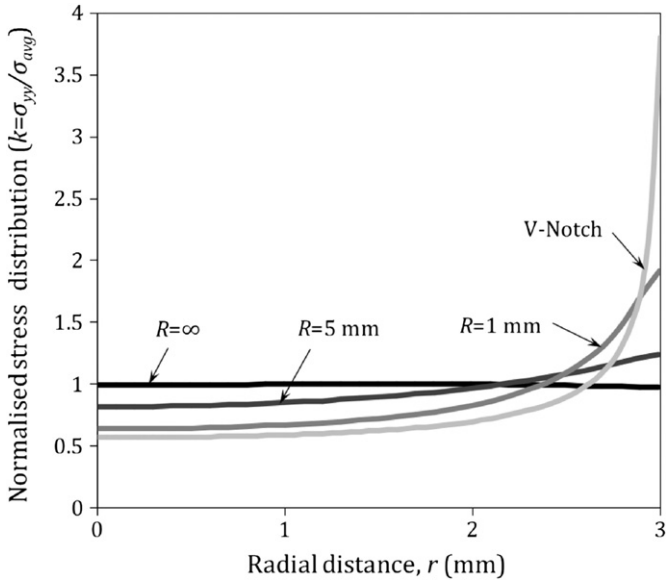

Fig. 6. Variation in normalised stress distributions ($k=\sigma_{yy}/\sigma_{avg}$) in the notched specimens with notch geometry.

reduced integration) in Abaqus/Standard 6.9. Geometric non-linear analyses were performed using a linear-elastic material behaviour.

Although the adhesive used in the current study is a toughened epoxy with hollow glass microspheres of different sizes, it was assumed to be homogenous with isotropic material properties to simplify the analyses. The Young's modulus and Poisson's ratio of the adhesive were assumed to be 2000 MPa and 0.4, respectively. The axisymmetric model used for analysing a V-notched specimen is shown in Fig. 5 as an example. Axisymmetric displacement boundary conditions were applied to the model (*i.e.* the boundary along $r=0$ and the boundary along $y=0$ in Fig. 5). A finer mesh was employed near the notch—with a typical element size of 0.1 mm × 0.1 mm. An axial displacement was applied and the stress distribution near the notched region was analysed.

Numerical analyses were performed for four different notch geometries (*i.e.* for $R=\infty$, $R=5$ mm, $R=1$ mm and V-notch). The influence of the notch geometry on the stress distribution is shown in Fig. 6. A normalised stress parameter—defined as the ratio of the axial stress to the average axial stress, $k=\sigma_{yy}/\sigma_{avg}$—was used to show the stress concentrations. It is seen from Fig. 6 that the normalised stress parameter increases along the radial direction and attains a maximum value (which is the stress concentration factor, K) at the notch tip. Moreover, the normalised stress contours for the four notch geometries is shown in Fig. 7. Similarly, the influence of the notch geometry on the stress triaxiality is shown in Fig. 8. The stress triaxiality—defined as the ratio of the hydrostatic stress to the von Mises stress, $\eta=-p/\sigma_{Mises}$—was used to show the triaxial stress states. In Fig. 8, it is shown that the stress triaxiality varies with notch geometry and attains a maximum value for a V-notch. Moreover, the stress triaxiality contours for the four notch geometries is shown in Fig. 9. The stress concentration factors (K) and the maximum stress triaxiality (η_{max}) near the notch tip are given in Table 1 for the four notch geometries. In the case of a V-notch, the adhesive was exposed to a combination of high stress

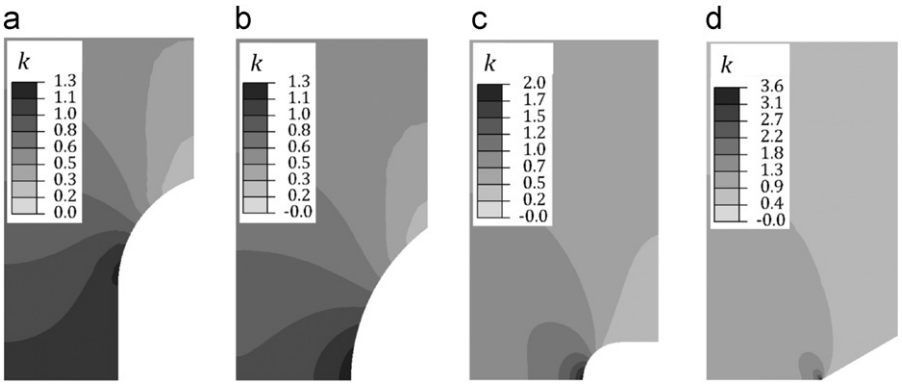

Fig. 7. Normalised stress contours ($k=\sigma_{yy}/\sigma_{avg}$) in the notched specimens.

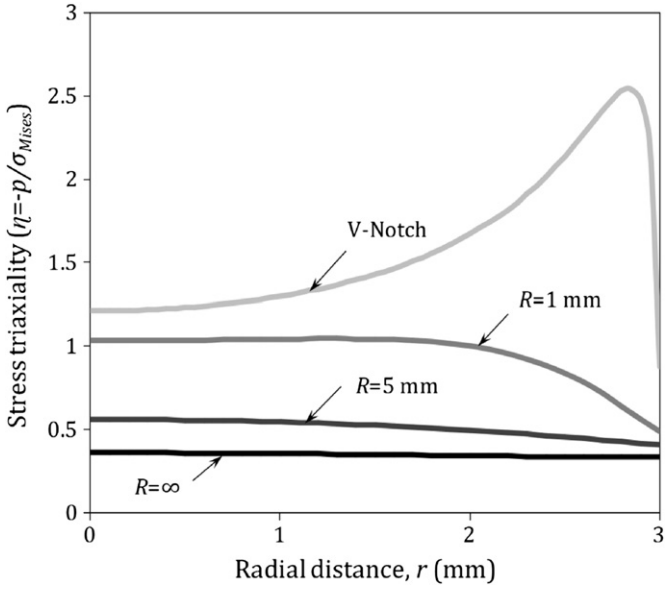

Fig. 8. Variation in stress triaxiality ($\eta=-p/\sigma_{Mises}$) in the notched specimens with notch geometry.

concentration (3.67) and high stress triaxiality (2.53)—suggesting that high radial stresses were induced with high axial stresses.

4. Experimental work

Cylindrical bulk adhesive specimens were tested in tension using a purpose-built test setup. Digital image correlation (using high magnification lens) was employed to analyse surface strains for specimens with notch radius $R=\infty$. Strain-rate and stress triaxiality dependent tensile tests were conducted. Fracture surfaces were examined using optical and scanning electron microscopy to identify micro-failure patterns.

4.1. Test setup

Tensile tests were conducted on the notched specimens in a tensile testing machine (Tinius-Olsen) with a 25 kN capacity load cell. Purpose-built steel chuck grips with split shoulders and pins were employed to accurately align the specimens and transfer applied loads (see Fig. 10a). The contact stresses (σ_a)—induced between the chuck grips and the hollow aluminium cylinders—transfer applied loads to the notched regions as shown in Fig. 10b. Moreover, the bond strength at the internal surface of the hollow aluminium cylinder provides shear resistance (through mechanical interlocking and bonding) to effectively transfer the applied loads to the bulk adhesive.

4.2. Tensile tests with digital image correlation

Initially, tensile tests were conducted on three notched specimens with $R=\infty$ (see Fig. 3a). To monitor the surface strain evolution, two-dimensional digital image correlation was used (Strain Master from La Vision, Germany). A high magnification zoom lens (Navitar 6000) was added to a CCD camera to focus a small surface area near the notch (approximately 1.2 mm × 3.5 mm). It was approximated as a flat surface for the image correlation. The notched region was speckled with a random pattern (black spackles on white background) using acrylic paint with an air brush (Badger 200-3). A small region (1.15 mm × 2.25 mm) was masked and post-processed to estimate surface displacements and strains with increased load levels. The speckled surface (with the area of interest) and the axial surface strain evolution obtained at three different load levels (1.0 kN, 1.5 kN and 1.9 kN) are shown in Fig. 11.

The load–displacement and stress–strain curves are shown in Figs. 12a and b, respectively. The stress and strain data in Fig. 12b are the average stress at the notched region and the average strain obtained from the digital image correlation, respectively. The surface strain distribution obtained prior to failure (strain contour at 1.9 kN in Fig. 11) indicate patches of strain gradients. It is thought that these strain gradients could have been induced by either the surface undulations introduced during notching or the hollow glass microspheres present in the adhesive.

The mechanical properties obtained from the tensile tests on the notched specimens with $R=\infty$ are given in Table 2. From the three tests conducted on identical specimens, an average failure load of 1.96 kN (with a standard deviation of 0.031) was found. The average axial stress (σ_{avg}) and axial surface strain (ε_{avg}) in the notched region prior to failure were 69.68 MPa and 3.82%, respectively.

4.3. Strain-rate and stress triaxiality tests

Tensile tests were conducted on the notched specimens to investigate the tensile fracture of the adhesive for different strain-rates and triaxial stress states. To examine the rate-dependent tensile behaviour, tests were conducted on the notched specimens with 5 mm notch radius at three different rates—with a hundred fold increase (0.1, 1.0, 10.0 mm/min). Furthermore, the influence of triaxial stress states on the fracture behaviour was investigated by testing the notched specimens with three

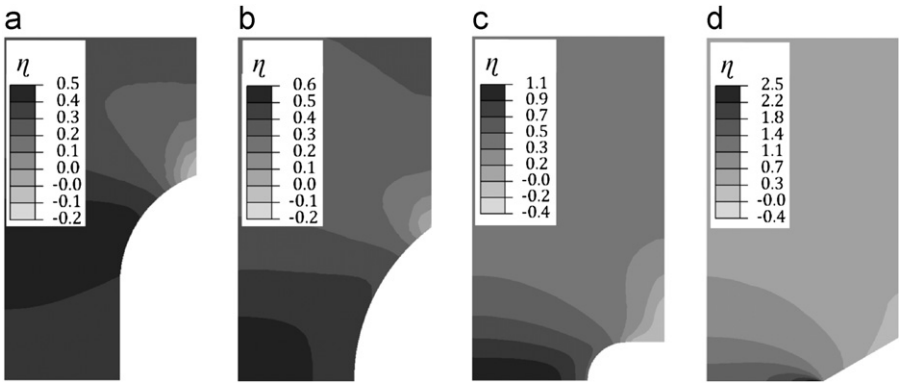

Fig. 9. Stress triaxiality contours ($\eta = -p/\sigma_{Mises}$) in the notched specimens.

Table 1
Stress concentration factors and stress triaxiality values in the test specimens.

Notch radius (mm)	Stress concentration factor (K)	Maximum stress triaxiality (η_{max})
$R=\infty$	1.00	0.33
$R=5$	1.24	0.55
$R=1$	1.91	1.03
V-notch	3.67	2.53

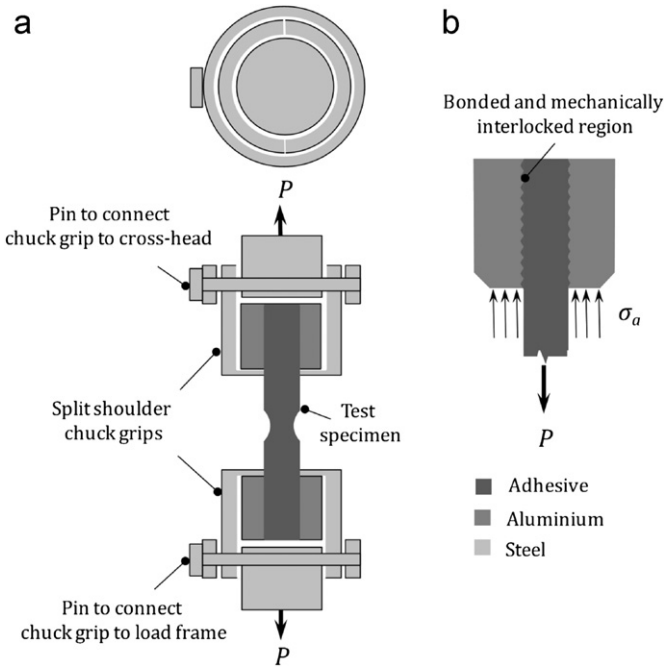

Fig. 10. Purpose-built tensile test setup: (a) chuck grips with split shoulders and pins and (b) load transfer mechanism through contact stresses induced at the surface of aluminium hollow cylinder.

different notch radii (5 mm, 1 mm and 0.02 mm)—at a constant displacement rate of 1.0 mm/min.

In Table 3, the data obtained from the tensile tests on the notched specimens with 5 mm notch radius is shown. Three identical specimens were tested for each displacement rate. The failure loads were found to have increased with increased displacement rates. The maximum axial stresses at the notch tip just before failure were calculated using the stress concentration factor (K) given in Table 1. When compared to 0.1 mm/min rate, an increase of 20.04% in failure stress was found for 10.0 mm/min rate. This indicated that the tensile behaviour of the adhesive is sensitive to strain-rates within the tested range.

Similarly, three specimens were tested for three notch geometries ($R=5$ mm, $R=1$ mm and $R \approx 0.02$ mm). The experimental test data is given in Table 4. The failure loads were found to have decreased with decreased notch tip radius. However, the maximum axial stresses at the notch tip just before failure, which were calculated using the stress concentration factor (K) given in Table 1, showed a considerable increase in the failure stress with decrease in notch tip radius. When compared to the specimens with $R=5$ mm, an increase of 86.01% in the failure stress was found for the specimens with $R \approx 0.02$ mm. This indicated that the tensile behaviour of the adhesive is influenced by stress triaxiality. However, it is important to note that these comparisons were made using the numerical models with a linear-elastic material response. On the other hand, high axial stresses along with high stress triaxiality may trigger a non-linear material response and reduce the stress concentration near the notch tip.

4.4. Fractography

To understand the failure mechanisms and the influence of strain-rate and stress triaxiality on the adhesive, the fracture surfaces were examined using optical and scanning electron microscopy (JOEL JCM-5700). The fracture surfaces were cleaned using compressed air to remove surface debris and digital images of the entire fracture surfaces were taken using an optical stereo microscope. For scanning electron microscopy, the fracture surfaces are initially coated with gold (20 nm) to avoid charge accumulation.

The fracture surfaces obtained from the strain-rate dependent tests are shown in Fig. 13—comparing the fracture at 0.1 mm/min displacement rate (Fig. 13a) with the fracture at 10.0 mm/min displacement rate (Fig. 13b). Both the surfaces show mirror-mist-hackle patterns with some dark circular dots, which may either be hollow glass microspheres of different sizes or micro voids. However, a considerable difference in the surface roughness can be seen in the two fracture surfaces—with a larger hackle region in Fig. 13b.

The fracture surface shown in Fig. 13b was further examined using scanning electron microscope. The micrographs were taken at a 45° tilt to observe the surface step patterns. In Fig. 14a, the entire fracture surface is shown and the two locations (the mirror region and the hackle region) where micrographs were taken at a high magnification. The two micrographs are shown in Figs. 14b and c. In the mirror region, which represents a slow fracture process, debonded hollow glass microspheres were seen—forming cavities around the microspheres. Moreover, a broken hollow glass

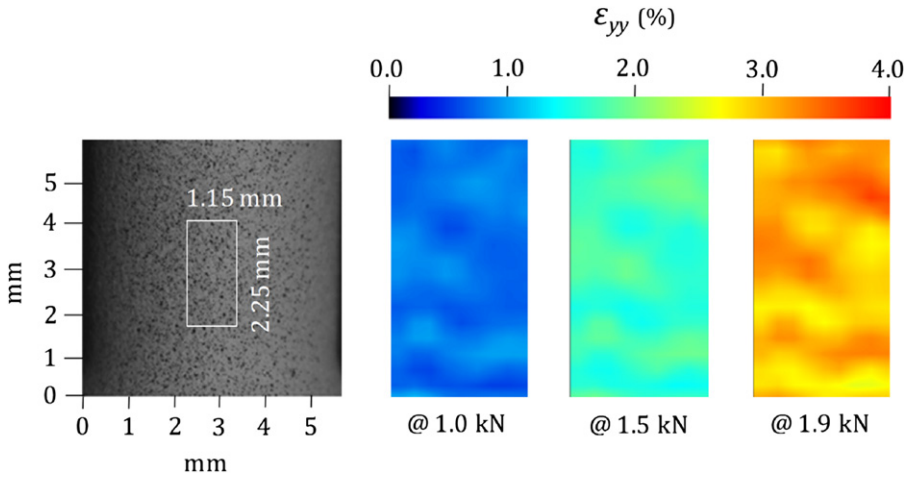

Fig. 11. Digital image correlation with high magnification lens for assessing the axial surface strains on the notched specimen with $R=\infty$.

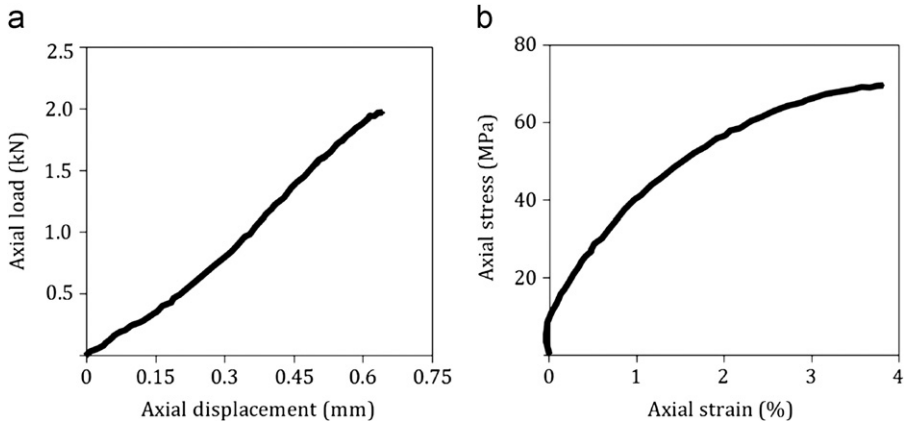

Fig. 12. Tensile behaviour: (a) the load–displacement curve and (b) the stress–strain curve.

Table 2
Tensile tests on the bulk specimens with $R=\infty$.

Notch radius (mm)	Displacement rate (mm/min)	Failure			Failure strain (%) ε_{avg}
		Load (kN)	SD	σ_{avg} (MPa)	
$R=\infty$	1.0	1.96	0.031	69.68	3.82

SD: Standard deviation; σ_{avg}: Average axial stress; ε_{avg}: Average axial surface strain.

Table 3
Strain rate dependent fracture behaviour of the adhesive.

Notch radius (mm)	Displacement rate (mm/min)	Failure			Variation (%) σ_{max}
		Load (kN)	SD	σ_{max} (MPa)	
$R=5$	0.1	1.752	0.073	76.83	–
$R=5$	1.0	1.970	0.054	86.39	+12.44
$R=5$	10.0	2.103	0.027	92.23	+20.04

SD: Standard deviation; σ_{max}: Maximum axial stress at failure.

microsphere with a characteristic tail [13] can be seen in Fig. 14b. However, in Fig. 14c, which is the fast fracture region, the surface pattern looks more random with no cavities around the hollow glass microspheres. A weak interface bond between the hollow glass microspheres and the bulk epoxy can also be seen with a smooth surface on the microspheres.

Table 4
Tri-axial stress state dependent fracture behaviour of the adhesive.

Notch radius (mm)	Failure			Variation (%) σ_{max}
	Load (kN)	SD	σ_{max} (MPa)	
$R=5$	1.970	0.054	86.39	–
$R=1$	1.694	0.035	114.43	+29.33
$R=0.02$	1.268	0.058	164.58	+86.01

SD: Standard deviation; σ_{max}: Peak axial stress at failure.

Similarly, the fracture surfaces obtained for two different notch geometries are shown in Fig. 13—comparing the fracture with a notch radius of 5 mm (Fig. 15a) with the fracture with a notch radius of 0.02 mm (Fig. 15b). A ring of stress-whitened area can be seen in Fig. 15b—with no or negligible stress-whitened area in the mirror region in Fig. 15a. This suggests that considerable local plasticisation of the adhesive occurred near the notch tip in Fig. 15b with high axial stresses accompanied by high stress triaxiality.

The fracture surface shown in Fig. 15b was further examined using scanning electron microscope. The micrographs were taken normal to the fracture to observe the surface features. Three micrographs—which were taken from mirror, mist and hackle regions, respectively—are shown in Fig. 16. In the mirror region

(see Fig. 16a), the hollow glass microspheres were debonded from the bulk epoxy and a step pattern was formed on the surface. But, in the mist region (see Fig. 16b), crack pinning mechanism was found with no or limited cavitation around the microspheres—indicating that microspheres influenced the local micro crack propagation by bowing the crack front [13]. Moreover, as shown in Fig. 16c, a fast fracture pattern with complex step formation and no cavitation around the debonded microspheres was found in the hackle region.

5. Discussion

From numerical modelling and experimental testing of circumferentially notched specimens, it was observed that strain-rate and stress triaxiality influenced the tensile behaviour of the adhesive by changing the failure mechanisms. Stress-whitening was found in the mirror region at high axial stresses accompanied by high stress triaxiality ($\eta > 1.0$).

It is known that in adhesively bonded joints, *e.g.* single lap joint, high shear and peel stresses are induced near the adhesive fillet region [2]. In the tensile failure of single lap bonded joints, cracks initiate in the fillet regions and propagate quickly along either the interface or the adhesive bondline—causing a sudden separation of the two adherends. This suggests that a complex material model, which accounts for both stress triaxiality and strain-rate effects, may be required to numerically predict the tensile failure of single lap bonded joints.

To estimate the stress triaxiality near the fillet region of a representative single lap joint, a two-dimensional plane strain model was used for a quasi-static analysis. A linear-elastic material response was assumed for adhesive and adherend materials. For the adherend (aluminium), the elastic modulus and Poisson's ratio were assumed as 70 GPa and 0.3, respectively. Similarly, for the adhesive, the elastic modulus and Poisson's ratio were assumed as 3 GPa and 0.4, respectively. The following dimensions were considered in the model: (a) a bondline thickness of 200 μm, (b) an adherend thickness of 2 mm and (c) an overlap of 25 mm. Moreover, an ideal interface, which can transfer any amount of stress, was assumed. Using plane strain elements (CPE4) in Abaqus/Standard 6.9, a quasi-static stress analysis was performed and the stress triaxiality distribution near the fillet region was estimated. The displacement boundary conditions and the mesh density used are shown in Fig. 17. The stress triaxiality contour near the fillet, given in Fig. 17, shows that high stress triaxiality ($\eta > 1.4$) exists near the fillet (at the embedded corner of the adherend). This suggests that the *in-situ* adhesive experiences high stress triaxiality—similar to the process zone in the bulk specimen with a notch radius of less than 1 mm. This, in turn, shows that circumferentially notched bulk specimens can provide material properties that can be used to develop predictive models for adhesively bonded joints.

6. Conclusions

A two-part epoxy paste adhesive—toughened with hollow glass microspheres—was used to investigate the influence of strain-rate and stress triaxiality on the tensile fracture behaviour. Cylindrical bulk adhesive specimens were manufactured with injection moulding and circumferential notches were introduced using a lathe machine. Strain-rate tests were conducted at three different displacement rates (0.1 mm/min, 1.0 mm/min and

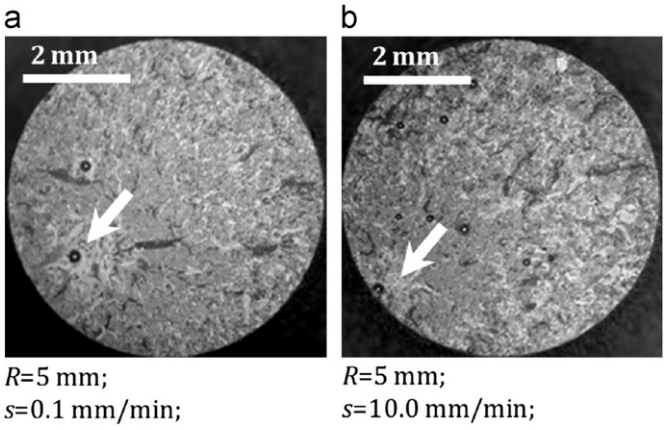

Fig. 13. Comparison of the fracture surfaces: (a) at 0.1 mm/min and (b) at 10.0 mm/min.

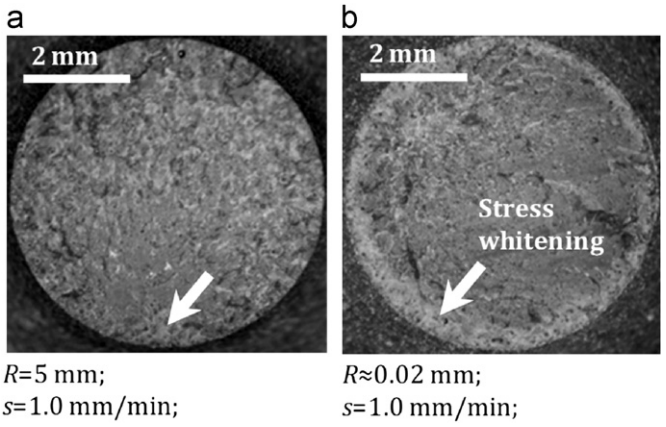

Fig. 15. Comparison of the fracture surfaces: (a) with $R = 5$ mm and (b) with $R \approx 0.02$ mm.

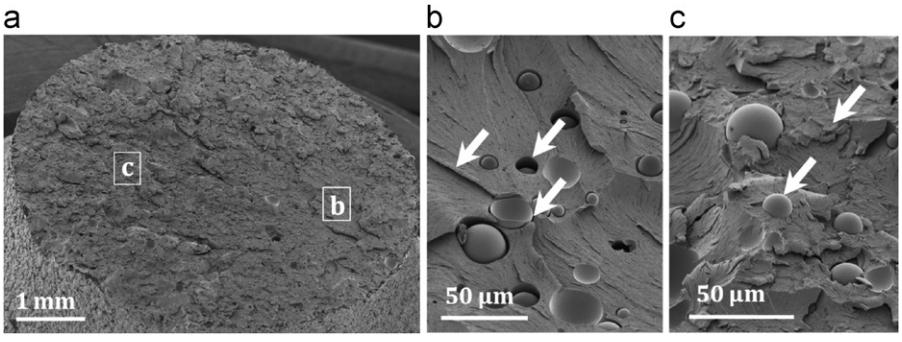

Fig. 14. Scanning electron microscopy: (a) fracture surface obtained at 10.0 mm/min displacement rate, (b) surface features in the mirror region and (c) surface features in the hackle region.

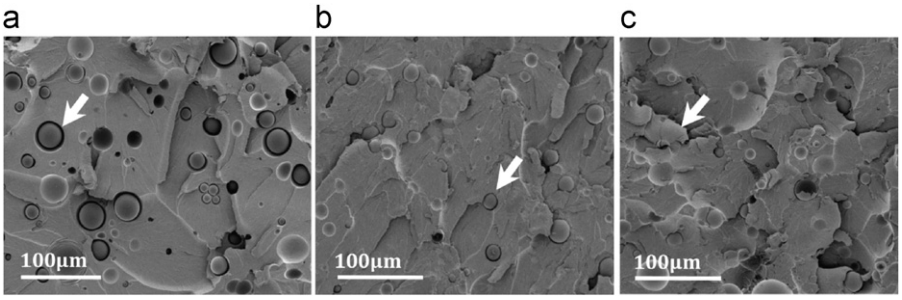

Fig. 16. Micrographs from the fracture surface obtained from a V-notch specimen: (a) the mirror region, (b) the mist region and (b) the hackle region.

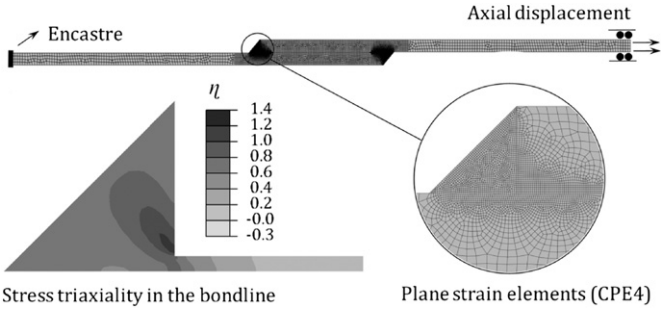

Fig. 17. Analysis of stress triaxiality near the adhesive fillet region in a single lap joint.

10.0 mm/min) and stress triaxiality tests were performed using different notch geometries ($R=\infty$, $R=5$ mm, $R=1$ mm and $R\approx 0.02$ mm). Using optical and scanning electron microscopy, fracture surfaces were examined to identify different failure mechanisms involved. The following key observations/conclusions are made:

- Cylindrical specimens were manufactured using injection moulding from a paste adhesive with no or limited void formation.
- Tensile tests conducted on the toughened adhesive revealed an increase in failure stress with increasing strain-rates (see Table 3). Moreover, an increase in failure stress was found with increasing stress triaxiality (see Table 4).
- Microsphere debonding with cavitation and step formation between microspheres were found in the slow fracture regions (i.e. the mirror-mist region), as shown in Fig. 14b. Furthermore, random step patterns with no or limited cavitation around the debonded microspheres were seen in the fast fracture (i.e. the hackle region), as shown in Fig. 14c.
- Stress-whitening—with cavitation around the debonded microspheres—was observed near the notch tip with high stress triaxiality. Crack pinning mechanism was found in the mist region, but without stress-whitening.
- Tensile tests on circumferentially notched bulk specimens can provide material properties as a function of strain-rate and stress triaxiality, which can be useful to develop predictive models for adhesively bonded joints.

Acknowledgements

The authors would like to acknowledge (a) Enterprise Ireland for research funding, (b) Mr. Paddy Kelly and Mr. Brian Nestor for manufacturing tools and (c) Ms. Emma Platt for bulk specimen preparation and testing at the University of Limerick, Ireland.

References

[1] Higgins A. Adhesive bonding of aircraft structures. Int J Adhes Adhes 2000;20(5):367–76.
[2] Adams RD, Comyn J, Wake WC. Structural adhesive joints in engineering. London: Chapman & Hall; 1997.
[3] da Silva LFM, Carbas RJC, Critchlow GW, Figueiredo MAV, Brown K. Effect of material, geometry, surface treatment and environment on the shear strength of single lap joints. Int J Adhes Adhes 2009;29(6):621–32.
[4] Lilleheden L. Mechanical properties of adhesives in situ and in bulk. Int J Adhes Adhes 1994;14(1):31–7.
[5] Jeandrau JP. Intrinsic mechanical characterization of structural adhesives. Int J Adhes Adhes 1986;6(4):229–31.
[6] Lees DE, Hutchinson AR. Mechanical characteristics of some cold-cured structural adhesives. Int J Adhes Adhes 1992;12(3):197–205.
[7] Zheng S, Ashcroft. IA. A depth sensing indentation study of the hardness and modulus of adhesives. Int J Adhes Adhes 2005;25(1):67–76.
[8] da Silva LFM, Adams RD. Measurement of the mechanical properties of structural adhesives in tension and shear over a wide range of temperatures. J Adhes Sci Technol 2005;19(2):109–41.
[9] Duan K, Hu X, Mai YM. Substrate constraint and adhesive thickness effects on fracture toughness of adhesive joints. J Adhes Sci Technol 2004;18(1):39–53.
[10] Pardoen T, Ferracin T, Landis CM, Delannay F. Constraint effects in adhesive joint fracture. J Mech Phys Solids 2005;53:1951–83.
[11] Wang CH, Rose LRF. Determination of triaxial stresses in bonded joints. Int J Adhes Adhes 1997;17:17–25.
[12] Imanaka M, Fujinami A, Suzuki Y. Fracture and yield behaviour of adhesively bonded joints under triaxial stress conditions. J Mater Sci 2000;35:2481–91.
[13] Lee J, Yee AF. Inorganic particle toughening I: micro-mechanical deformations in the fracture of glass bead filled epoxies. Polymer 2001;42:577–88.
[14] Lee J, Yee AF. Inorganic particle toughening II: toughening mechanisms of glass bead filled epoxies. Polymer 2001;42:589–97.
[15] Lee J, Yee AF. Fracture of glass bead/epoxy composites: on micro-mechanical deformations. Polymer 2000;41:8363–73.
[16] Park SJ, Jin FL, Lee C. Preparation and physical properties of hollow glass microspheres-reinforced epoxy matrix resins. Mater Sci Eng A 2005;402:335–40.
[17] Xu CC, Siegmund T, Ramani K. Rate-dependent crack growth in adhesives-II. Experiments and analysis. Int J Adhes Adhes 2003;23(1):15–22.
[18] Pohlit DJ, Dillard DA, Jacob GC, Starbuck JM. Evaluating the rate-dependent fracture toughness of an automotive adhesive. J Adhes 2008;84:143–63.
[19] Banea MD, de Sousa FSM, da Silva LFM, Campilho RDS, de Pereira AMB. Effects of temperature and loading rate on the mechanical properties of a high temperature epoxy adhesive. J Adhes Sci Technol 2011;25(18):2461–74.
[20] Tiejun W, Kishimoto K, Notomi M. Effect of triaxial stress constraint on the deformation and fracture of polymers. Acta Mech Sin 2002;8(5):480–93.
[21] Asp LE, Berglund LA, Gudmundson P. Effects of a composite-like stress state on the fracture of epoxies. Compos Sci Technol 1995;53:27–37.
[22] Kody RS, Lesser AJ. Deformation and yield of epoxy networks in constrained states of stress. J Mater Sci 1997;32:5637–43.
[23] Kishi H, Shi YB, Huang J, Yee AF. Ductility and toughenability study of epoxy resins under multi-axial stress states. J Mater Sci 1998;33:3479–88.
[24] da Silva LFM, Ochsner A. Modelling of adhesively bonded joints. Berlin: Springer-Verlag; 2008.
[25] Alves M, Jones N. Influence of hydrostatic stress on failure of axisymmetric notched specimens. J Mech Phys Solids 1999;47:643–67.
[26] Noda NA, Sera M, Takase Y. Stress concentration factors for round and flat test specimens with notches. Int J Fract 1995;17(3):163–78.
[27] Tlilan HM, Al-Shyyab AS, Jawarneh AM, Ababneh AK. Strain concentration factor of circumferentially V-notched cylindrical bars under static tension. J Mech 2008;24(4):419–27.
[28] Ting SKM, Williams JG, Ivankovic A. Characterisation of the fracture behaviour of polyethylene using measured cohesive curves: I: effects of constraints and rate. Polym Eng Sci 2006;46:763–77.